THE PENNSYLVANIA STATE UNIVERSITY
SCHREYER HONORS COLLEGE

DEPARTMENT OF METEOROLOGY

HO_x MEASUREMENTS TAKEN DURING THE SOAS 2013 CAMPAIGN AND THEIR IMPLICATIONS FOR HO_x MODELING

PHILIP FEINER
FALL 2014

A thesis
submitted in partial fulfillment
of the requirements
for a baccalaureate degree
in Meteorology
with honors in Meteorology

Reviewed and approved* by the following:

William Brune
Distinguished Professor of Meteorology
Thesis Supervisor
Honors Adviser

David Miller
Research Associate
Department of Meteorology
Faculty Reader

*Signatures are on file in the Schreyer Honors College.

Abstract

OH and HO $_2$, collectively referred to as HO_x plays a key role in removing many pollutants from the atmosphere. Attempts to model HO_x have proven to be troublesome in forested, low NO_x environments as model predictions rarely match measured values. Some scientists feel that this discrepancy comes from a poor understanding of forest oxidation chemistry. Other work has presented the possibility that this discrepancy is due to an interference signal affecting HO_x measurements in the field. This paper examines HO_x measurements from the Southern Oxidant and Aerosol Study (SOAS) and how they compare to calculated model values. SOAS represents a low NO_x environment with many supporting measurements that can be used to constrain the relevant chemistry. The results imply that we possess an adequate understanding of the isoprene oxidation chemistry and that other instruments making measurements by a similar method may be affected by an unknown interference signal.

Table of Contents

List of Figures

Acknowledgements

I would like to thank Dr. Brune for his guidance and help in making all of this possible for me. In addition I'd like to thank David Miller for answering a thousand questions a day every day and for his advice on everything from MATLAB to life decisions.

Thanks also to my family and friends for standing by me through the madness of grad school.

Chapter 1

Introduction

Atmospheric oxidation serves many important roles in our atmosphere that are important to mankind. It affects the climate by having an influence on the concentrations of several species that absorb infrared radiation like methane and ozone. It is also the driving factor in determining air quality. Oxidation processes are responsible for converting many volatile pollutant chemical species into other, more water-soluble species that can be scrubbed from the atmosphere by rain or dry deposition onto surfaces.

The oxidation chemistry taking place in and around forested environments is particularly important in determining the global concentrations of many chemical species. Given that forested environments cover such a large area of the Earth's surface (Hansen et al. (2003)), their effects on global chemistry are far reaching and having a proper understanding of these processes is vital to modeling global chemistry correctly.

While oxidation drives atmospheric processes, many atmospheric species containing oxygen have relatively low reactivity as oxygen often forms strong chemical bonds that are not easily broken. However, one atmospheric constituent, the hydroxyl radical (OH), is extremely reactive. Between its high reactivity and its ability to be produced quickly and in large numbers, the hydroxyl radical acts as the atmosphere's main oxidizing agent. The hydroxyl radical and the closely related hydroperoxyl radical (HO_2) are collectively called HO_x, which has important roles in the production of ozone and small aerosol particles. Thus, knowing its characteristics and concentrations is key to understanding atmospheric chemistry in general (Seinfeld and Pandis, 2006).

1.1 HO_x Chemistry

Globally, OH radicals are produced primarily through the photofragmentation of ozone by ultraviolet sunlight into molecular oxygen and excited state oxygen atoms (reaction 1.1). Some of these excited state oxygens collide with nitrogen and oxygen molecules to become ground state oxygen, eventually reforming ozone. However, about ten percent of these atoms are able to react with water vapor, forming two hydroxyl radicals (reaction 1.2).

$$O_3 + h\nu \longrightarrow O_2 + O(^1D) \quad \{1.1\}$$

$$O(^1D) + H_2O \longrightarrow 2\,OH \quad \{1.2\}$$

However, this reaction sequence is not the only source of OH in the troposphere. OH can also be formed through the direct photolysis of other molecules like HONO, H_2O_2, and CH_3OOH. OH is also a product in reactions of ozone with volatile organic compounds (VOCs) that contain double bonds between carbon atoms. However, photolysis of ozone is still the primary global source.

OH reacts with many atmospheric trace gases but not with any of the main atmospheric constituents N_2, O_2, CO_2, and H_2O. OH will however, react with other volatile chemical species it encounters in the atmosphere. When OH reacts with a volatile compound, it will either extract a hydrogen from the molecule, or it may end up adding itself to the molecule. Either way, the reaction with OH goes on to form a molecule with an odd number of electrons surrounding it, also known as a radical. Radicals tend to be reactive themselves and quickly react with another molecule or with other radicals.

HO_2 radicals are formed through the photolysis of formaldehyde, the reaction of OH with CO, and with VOCs in the presence of NO and NO_2 (NO_x). OH oxidation of VOCs initiates reactions that form organic peroxy radicals, RO_2, where R represents an organic group. These peroxy radicals react with ambient NO to produce NO_2 and recycle HO_x. This recycling of OH and HO_2 is most efficient for intermediate NO_x concentrations. The opposite is true in low NO_x environments where a lack of NO_x limits the amount of HO_x that can be recycled (Monks, 2005). The reactions that produce and consume HO_x are fairly well understood, but the complexity of the organic chemistry and the competing reaction pathways between HO_x and NO_x make it difficult to determine the net HO_x production or loss in these oxidation sequences.

1.2 Past HO_x Measurements and Comparison with Models

Comparing measured and modeled HO_x values is of great interest to the atmospheric chemistry community. HO_x radicals have an extremely short lifetime in the atmosphere, on the order of a second for OH radicals and only about a minute for HO_2. As such, it exists in essentially a photochemical steady state with concentrations only being dictated by OH sources and sinks (Monks, 2005). Given that transport terms are typically longer than HO_x lifetimes, predicting HO_x levels accurately can be done using a photochemical box model. However, while OH measurements have been available since at least the mid 1980's, modeling has been held back by an inability to properly measure the major constraining factors needed to model HO_x (Rohrer et al., 2014). Over the past two decades, several *in situ* HO_x measurements have been made during field campaigns and then compared to model calculations. These campaigns have covered many different environments from the forests of the Amazon to the heavily polluted atmospheres of major cities like New York and Mexico City.

Comparing these results with model predictions has yielded mixed results that seem to depend upon the environment in which the data were collected. For measurements taken in urban, high NO_x environments, OH measurements have fared well compared to models, but HO_2 tends to be under-predicted (Kanaya et al., 2007). Many of the discrepancies between modeled and measured HO_x tend to depend on the concentration of NO that was measured. As NO concentrations increase, models have tended to perform more poorly in describing HO_2. The results of several campaigns have shown that HO_2 is under-predicted with this discrepancy growing larger as NO concentration does (Ren et al., 2003a). Comparing the modeled versus measured values for HO_2/OH also found an increasing discrepancy as NO increased, as the modeled ratio decreased

much faster than the measured did. However, measurements taken during MCMA-2013 in Mexico City did see better modeled versus measured agreement for this ratio (Shirley et al., 2006). Attempts to characterize the overall HO_x budget in these environments have had limited success. OH production was under-predicted during SOS in Nashville but over-predicted in Mexico City and in New York during PMTACS-NY2001 (Ren et al., 2003a; Shirley et al., 2006; Martinez et al., 2003).

In more rural environments, rich with biogenic volatile organic compounds (BVOCs) and low in NO_x, agreement between modeled and measured OH values has rarely been observed (Tan et al., 2001; Faloona et al., 2000; Whalley et al., 2011). HO_2 modeling has been more successful, though, a recent paper by Fuchs et al. (2011) has uncovered a possible interference in HO_2 measurements due to alkene and aromatic organic peroxy radicals (RO_2s). Even when taking this interference into account, HO_2 has been more successfully modeled than OH in forests.

The struggle with properly modeling OH in these environments relates to two primary factors. First, the levels of NO_x have a notable influence on the overall agreement between models and measurements. This agreement is especially apparent in urban campaigns, but even in more rural efforts, the models generally perform well on days with high concentrations of NO_x. Lu et al. (2013) provides an excellent example of this behavior for a field study in a rural area just south of Beijing. On days in which the prevailing winds came from the south, the site was exposed to air masses lacking anthropogenic influences and low in NO_x. On these days OH concentrations were under-predicted by a factor of 2.4. However, on days in which the wind came out of the north, NO_x values increased and agreement between the measurements and models improved. The same group, on a campaign in the Perl River Delta, saw strong agreement between measurements and model outputs on days in which NO concentrations exceeded 1 ppb. However, their model under-predicted OH by a factor of 8 when the NO values dropped below 0.02 ppb (Lu et al., 2012). This behavior was explored more closely in a recent paper from Rohrer et al. (2014) which shows how over-prediction of OH decreases as a function of NO_x. This better agreement for OH with high NO_x values is a feature of many other field studies as well (Ren et al., 2003b).

A second factor that seems to affect the modeled versus measured OH is the ambient concentration of isoprene and other biogenic volatile organic compounds (BVOCs). The largest source of OH reactivity over many of the world's forests comes from isoprene, and its presence tends to be associated with poor measured/modeled OH agreement (Faloona et al., 2000; Tan et al., 2001; Ren et al., 2008; Whalley et al., 2011). There are several examples of OH under-prediction in high isoprene environments, but its effect was especially notable during the aircraft-based INTEX-A campaign. During the campaign, the discrepancy between modeled and measured OH was usually small, but the discrepancy increased as the aircraft passed over isoprene-rich forests (Ren et al., 2008). All of the OH measurements that are substantially larger than modeled were made with instruments that used laser induced fluorescence (LIF) detection of OH.

One notable exception to this behavior came during the BEARPEX campaign which took place over a California forest (Mao et al., 2012). This campaign made use of a chemical removal technique for measuring OH that will be discussed later in this paper. Making use of this technique, measurements of OH were taken which showed a good agreement with the models while the old method still produced OH measurements that were 2.5 times modeled OH. (Mao et al., 2012) Another similar result was produced above a boreal forest in southern Finland where OH measurements were successfully modeled as well (Hens et al., 2013). This forest had low NO_x, but the forest's emissions were not isoprene but instead, more complex terpenes.

These results point to some sort of problem related to low NO_x high BVOC environments,

though the specific nature of the problem is still unclear. This discrepancy may indicate a poor understanding of the underlying chemistry and suggests that more OH is being produced by this chemistry than is currently contained in the models. This OH discrepancy has led to much greater scrutiny of the isoprene chemistry and investigation into the possibility that an unknown mechanism exists to recycle OH back into the atmosphere (Goliff et al., 2013). An alternative is that LIF measurements are susceptible to an as of yet unknown interference in low NO_x environments and that this interference is causing the discrepancy in measured and modeled OH (Mao et al., 2012; Hens et al., 2013).

OH reactivity, the inverse of the lifetime of OH, provides an interesting diagnostic tool to determine the completeness of the measurement suite from a given campaign. Another way to view the OH reactivity is the product of the reaction rate for a gas with OH and the concentration of the gas, summed over all gases that react with OH. A comparison of the OH reactivity calculated from the measured OH reactants and reactivity measured directly shows if some of the important OH reactants were not measured. In previous campaigns, it has often proven difficult to match the measured OH reactivity with calculated OH reactivity (Di Carlo et al., 2004). This is especially true in forested environments, likely due to their complex chemistry.

1.3 Motivation

Because environments with high levels of biogenic volatile organic compounds and low levels of NO_x are widespread and globally important, discovering the true source of the modeled versus measured OH discrepancy is essential to accurately model the atmospheric chemistry in these environments and globally. The goal of this paper is to examine this question using field data collected during the Southern Oxidant and Aerosol Study, conducted in summer 2013 in an isoprene-rich forest in central Alabama. The measurements will be compared to the output of a widely used photochemical box model. The effects and potential benefits of the recently discovered RO_2 interference on HO_2 measurements will also be explored with the hope that this measured interference signal can be used as a proxy measurement for ambient RO_2. The large number of measured atmospheric species during SOAS and our improved measurement capabilities for OH, HO_2 and RO_2 provide powerful constraints on the isoprene chemistry.

Chapter 2

Instrumentation and Data Collection

2.1 Penn State's Ground Based Tropospheric Hydrogen Oxides Sensor and OH Reactivity Instrument

Penn State's Ground Based Tropospheric Hydrogen Oxides Sensor (GTHOS) measures atmospheric HO_x concentrations through the use of a Fluorescent Assay of Gas Expansion, or FAGE, technique which has been described in several previous papers (Faloona et al., 2004; Mather et al., 1997; Stevens et al., 1994). A schematic diagram in Figure 2.1 shows a cross section of the instrument. Sampled air is pulled into the instrument through a small pinhole inlet. As the air moves through the instrument interior, it flows through the path of a laser beam that is tuned to an absorption line of OH. OH in the sample air absorbs energy from the laser and moves to an excited state. The excited-state OH then fluoresces and this fluorescence is ultimately measured by the instrument and used to infer the ambient concentration of OH. Sample air then continues to the HO_2 measurement axis where HO_2 is converted by chemical reaction with NO to OH and measured in the same manner as OH in the first axis.

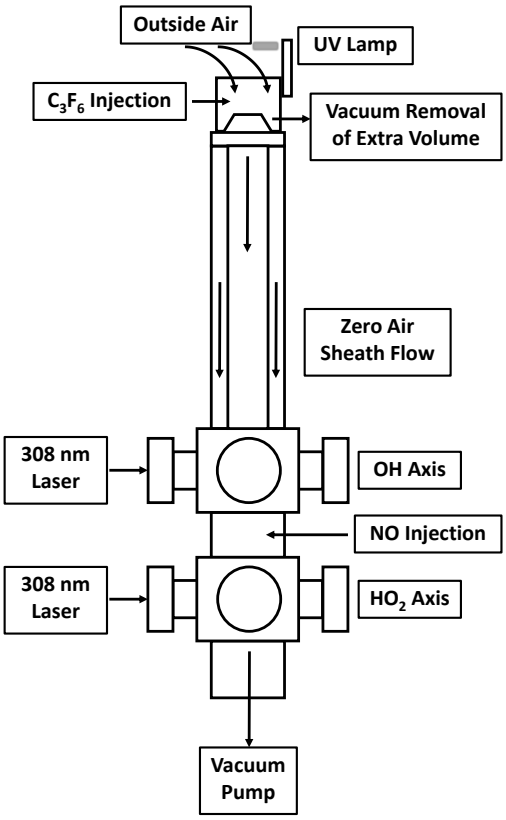

Figure 2.1: This schematic diagram shows a cross section of GTHOS setup as it was used to take measurements during SOAS. C_3F_6 was injected through six 0.25 mm needles which were pointed towards the center of the inlet. Attached just above the inlet was a mercury lamp used for daily testing of the C_3F_6 injection system's effectiveness.

The $Q_1(2)$ OH absorption line used in this measurement technique is at a wavelength of 308 nm. Because lasers at this wavelength and with the proper power output are not manufactured, a standard frequency-doubled Nd:YAG laser is used and its wavelength is then converted to 308nm. In the case of GTHOS, this system uses a tunable dye laser pumped by a 532nm Spectra Physics laser to produce 616nm light. The dye laser frequency is then doubled to produce the 308nm laser. The laser wavelength can be tuned using an etalon which is controlled by a stepper motor. To ensure that the laser wavelength remains on the OH absorption line, a small percentage of the total laser power is passed to a reference cell. Within the reference cell, a photo multiplier tube measures the florescence signal from a large OH source, in this case the thermolysis of H_2O by a hot filament wire.

Ambient air containing OH radicals is brought into the instrument through the pinhole (1 mm diameter) and passed through the path of the laser. The resulting fluorescence is then measured by a microchannel plate detector. In order to increase the absorption of the laser light by the OH, the laser is bounced back and forth through the measurement axis between 32 and 36 times with a White Cell (White, 1942). The actual OH signal is found by first tuning the dye laser to a

wavelength off of the OH absorption line to measure any background signal that may be present. Then the laser is tuned to the absorption line and the difference between the two signals is assumed to be the signal of OH fluorescence. We refer to this method of OH detection as OH_{wave}. OH_{wave} data can be collected at a time resolution of 20 seconds, though for SOAS it was collected at 30 second time intervals. A more detailed discussion of the standard OH measurement technique, as well as the technique used to measure HO_2 can be found in (Faloona et al., 2004)

When taking measurements, the inside of the detection system is pumped down to a near vacuum environment of between four and seven hPa. This low pressure is required for two main reasons. First, the excited state OH molecules can either fluoresce or return to the ground state by colliding into other atmospheric constituents like nitrogen, oxygen, and especially H_2O, a process referred to as quenching. Given that OH radicals undergoing quenching instead of florescence do not give off a photon which can be measured by the instrument, minimizing quenching is important to maximizing signal strength. Therefore, the lower molecule density is key as OH radicals that are excited are more likely to fluoresce to shed excess energy rather than be quenched. Second, the low particle density also slows the rate of oxidation chemistry taking place within the instrument. Slowing any active chemistry to a near stop allows the instrument to more accurately measure the true OH concentration of the atmosphere.

A second method for measuring OH was also used during SOAS. This method of detection involved injecting C_3F_6 into the sample air to scavenge OH before the air enters the pinhole (Mao et al., 2012). C_3F_6 reacts quickly with OH and does not absorb light around 308 nm and so is well suited for this purpose. By alternating times with C_3F_6 on and off, the concentration of OH is determined based on the difference in signal. C_3F_6 was added to the sample air through an injection system that was affixed to the top of the GTHOS inlet (Figure 2.1). While C_3F_6 was injected periodically, a constant N_2 flow of 1000 sccm was added through the injectors to promote mixing. The inlet add-on also contained a vacuum flow of 2000 sccm to improve the flow characteristics of air going into the inlet and to improve the mixing of C_3F_6 into the sampled air. To confirm that C_3F_6 was effectively removing OH, a UV lamp that produces copious OH was affixed to the outside of the instrument, just above the inlet. At least three set times a day, the lamp was turned on for a full cycle with C_3F_6 going off and on. This method allowed for a rough approximation of the conversion efficiency of the OH. We refer to this OH measurement method as OH_{chem}. OH_{chem} measurements consistently report lower concentrations of OH than the OH_{wave} measurements. For the purposes of this paper, the OH_{chem} measurement is assumed to be the true concentration of OH because this method is able to remove all of the OH produced by the external mercury lamp. OH interference (OH_{int}), the difference between OH_{wave} and OH_{chem} represents the interference causing this discrepancy and will also be presented with the results.

After the campaign, a more detailed analysis of OH_{chem} conversion efficiency was made in the lab to determine the detection sensitivity for OH. These experiments performed in the lab, as well as experiments performed in a subsequent chamber study, were used to determine conversion efficiency outside of the instrument. In addition, these experiments helped to characterize the internal conversion of any interference OH by C_3F_6 being brought into the instrument. These results were then used to develop the data processing software which produces the final OH dataset.

HO_2 measurements are also taken through a second measurement axis downstream of the OH measurement axis (Figure 2.1). Atmospheric HO_2 is converted to OH through reaction with NO injected into the sample air just above the HO_2 measurement axis (Reaction 2.3).

$$HO_2 + NO \longrightarrow OH + NO_2 \quad \{2.3\}$$

This converted HO_2 is then measured in the same manner as OH is measured in the first axis. However, when making HO_2 measurements through reactions with NO, RO_2 radicals formed by the oxidation of BVOCs can be a significant source of interference.

$$OH + RO \longrightarrow H_2O + R\cdot \quad \{2.4\}$$
$$R\cdot + O_2 \longrightarrow RO_2 \quad \{2.5\}$$

These organic peroxy radicals, formed by Reactions 2.4 and 2.5 can react with ambient NO to form more HO_2 in the atmosphere (Reactions 2.6 and 2.7). It is possible for this same reaction to take place within GTHOS, before the sampled air reaches the measurement axis. However, this reaction is undesirable within the instrument as the extra HO_2 produced in the reaction will be measured by the instrument as well, leading to a reported concentration higher than the ambient.

$$RO_2 + NO \longrightarrow RO + NO_2 \quad \{2.6\}$$
$$RO + O_2 \longrightarrow R'CHO + HO_2 \quad \{2.7\}$$

Previous efforts have been made to determine if this interference source could be significantly affecting the reported concentration of HO_2 (Ren et al., 2004). However, in chemicals tested previously, the reaction with O_2 (reaction 2.5) happened slowly enough that no additional HO_2 was produced in time to be converted into OH and measured. However, for RO_2 species formed from alkenes, such as isoprene, and aromatics, reaction 2.5 takes place at a much faster rate, producing HO_2 in a few milliseconds. Thus, this RO_2 interference is potentially problematic, especially in high isoprene environments like that of SOAS.

In order to check for interference from this source during SOAS, the flow rate of NO was ramped between several values. In the case of RO_2, the reaction rate with NO is different from the reaction rate between NO and HO_2 so by ramping NO, the interference signal can be identified and separated out from the true signal. In addition, lab work was done after SOAS to quantify the effects this interference had on measurements. This analysis will be discussed in greater detail in the next chapter.

2.1.1 GTHOS Calibration

To calibrate GTHOS, OH and HO_2 are created through the photolysis of water vapor in a system described in detail in Faloona et al. (2004). The calibration system makes use of ultra-zero air that is flowed through a bubbler of high purity H_2O. Water vapor concentration is recorded and the moistened air is passed by a mercury UV lamp emitting at 185 nm. Knowing the lamp flux, the water concentration and the period of time that the water was exposed to the 185 nm light, the OH and HO_2 concentrations of the calibration air can be calculated and the GTHOS measurement sensitivity can be determined. Like other similar LIF-FAGE instruments, GTHOS sensitivity

decreases slightly as ambient water concentration increases because water vapor is an effective quencher of the OH excited state. As such, the calibration process also includes measurements at several different water vapor amounts to ensure that the calibration is understood over the range of water vapor encountered in the atmosphere.

For all calibrations, the lamp flux is determined by at least two different methods. The first uses a NIST-calibrated photodiode to map the 185 nm flux at several positions within the calibration flow tube and then determine the average flux to which water vapor is exposed. The second method measures the amount of ozone produced by the photolysis of O_2 followed by the reaction between O and O_2 to produce ozone. The absolute O_2 cross section, which depends on the lamp characteristics, is determined by measuring the attenuation of 185 nm light in a small chamber of known length containing a known amount of O_2. These two methods give the same lamp flux to within 18%.

Calibrations were performed in the field during SOAS as well as after SOAS. However, the calibrations performed in the field were of a low quality due to high winds mixing ambient air and air from the calibration wand. As a result, the only calibrations applied to the final data were the ones performed in the lab setting, with some prior to the campaign, but most afterwards. A long history of calibrations and instrument changes shows that the calibrations are stable to within (10-15)% in periods where the instrument remained in the same configuration.

2.1.2 OH Reactivity Instrument

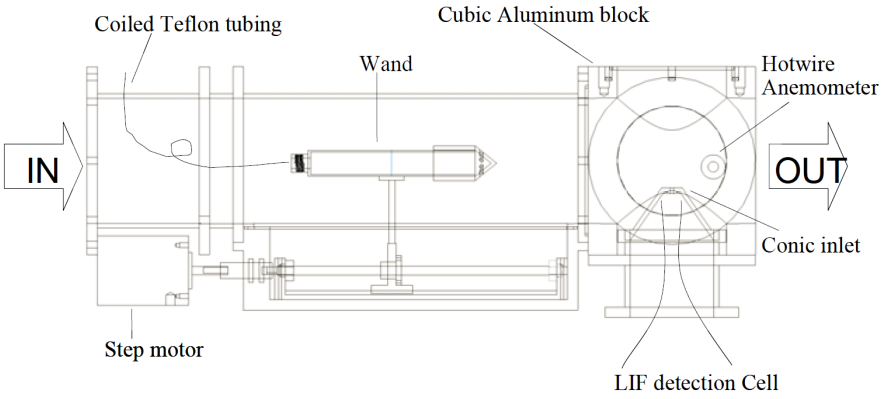

Figure 2.2: This schematic diagram shows a cross section of The OH reactivity instrument setup as it was used to take measurements during SOAS. Ambient air flows through the main tube while a movable OH source adds copious OH to the flow. The resulting OH signal is measured at the end of the tube and the difference in signal based on the location of the OH source can be used to determine OH reactivity. Figure from Mao et al. (2009).

For most field work, GTHOS also runs in conjunction with an instrument taking measurements of OH reactivity. The instrument, shown in Figure 2.2 and described in detail in Mao et al. (2009)

and Kovacs and Brune (2001) uses the discharge flow kinetics measurement method. A large volume of ambient air flows (160 LPM) through the central tube which has an inlet and OH measurement system nearly identical to the GTHOS system at the end of it. Prior to the measurement inlet, a movable OH source creates a large OH signal while moving closer to and farther away from the inlet to the HO_x detection cell. By analyzing the change in signal as the OH changes its distance from the inlet, the OH reactivity can be determined. For SOAS, measurements were taken every 30 seconds.

Calibrations for the OH reactivity instrument were performed by running zero air through the instrument to establish a zero. The zero was found to be 4.7 ± 2 s^{-1}. Next, gas mixtures with a known quantity of a common BVOC such as isoprene were added to the flow. The calculated OH reactivity was then compared to the measured OH reactivity in order to determine a calibration factor. Based upon tests this calibration factor was determined to be $1.06\pm$ (2σ confidence).

2.2 The Southern Oxidant and Aerosol Study

The Southern Oxidant and Aerosol Study (SOAS) was a 2013 campaign that was a part of the larger Southern Atmosphere Study (SAS) (Rugters). The primary mission of the campaign was to study the interactions between the forest biosphere and the atmosphere above it. Specifically, the campaign focused on the emissions of BVOCs, the oxidation chemistry they went through, and their eventual formation into secondary organic aerosols (SOAs). A better understanding of these processes has widespread applications, from improving the quality of regional pollution models to better predicting climate change. Data were collected for SOAS at several locations and on several platforms. The main SOAS site was in Brent, Alabama, but through cooperation with the SAS, data was also collected at two supersites in Look Rock Tennessee and Research Triangle Park, North Carolina. Several airborne platforms were also used, including the NSF/NCAR C-130, the NOAA P3, Purdue's Duchess aircraft, the Stony Brook Long-EZ and several sonde launches from the three ground sites.

2.2.1 Centreville SOAS Site

The main SOAS site was located just outside of Brent, Alabama, within the Talladega National Forest. The site was in a small clearing surrounded on all sides by a dense Southeastern mixed forest environment composed of both pine trees and broad leaf species such as oak. The canopy height of the forest at the site was between nine and twelve meters. The final site was chosen for several reasons. First, for the varied makeup of the forests which were similar in composition to many forests around the southeastern United States. Second, it is relatively isolated from anthropogenic influences but does experience anthropogenic influence, particularly from Birmingham 70 km to the Northeast and Tuscaloosa, 50 km to the Northwest. The Brent site had measurements situated in two main areas. The first area featured a grouping of trailers where most aerosol properties were measured. About one hundred meters away and slightly downhill from the main area, two trailers and an eighteen-meter scaffolding tower were erected. On top of the tower were the inlets for several gas-phase instruments and meteorological instruments. In addition, three full instruments were situated on top of the tower, namely: HO_x measurements from GTHOS, OH measurements from the University of California Irvine CIMS instrument, and VOC measurements from the Cal

Tech CIMS instrument. From June to mid-July of 2013, data were recorded from the Brent site by all of the participating groups.

2.2.2 GTHOS Setup During SOAS

In past field campaigns using GTHOS, the instrument has been split into three parts, with the detection axes on top of the tower, the vacuum pumps at the base of the tower, and the laser and electronics in a trailer near the tower. Long electrical cables connected the electronics to the detection system and long fiber optic cables carried the laser light from the laser to the detection axes. Most of the UV laser light was lost in these long cables so that the GTHOS detection sensitivity was severely degraded.

During SOAS, the entire GTHOS instrument was housed in a single container on top of the tower and only vacuum pumps were at the base of the tower. A large carrying case was constructed for the campaign which allowed the measurement axis, laser, computer system and OH reactivity instrument to sit together. Thus, the fiber optic cables could be quite short and the detection sensitivity obtained in the laboratory could be obtained in the field without the degradation of the long fiber optic cables. In addition, the constructed case also included an integrated climate control system which allowed the entire instrument to remain at a constant temperature throughout the course of the campaign. This constant climate control mitigated some of the subtle changes in the instrument's optics system that has caused the laser to drift out of optimum alignment in previous campaigns in which the temperature and relative humidity varied in the trailer that housed the laser. An inlet tube for the OH reactivity instrument was run from the inside of the container to the outside and then fastened so that it hung over the edge of the tower, allowing it to sample air from directly over the forest canopy while minimizing the influence of the tower itself.

2.3 Data Filtering and Corrections

The raw data collected were carefully examined in order to ensure that the final dataset was of the highest possible quality. To facilitate this goal, a filter was applied to the data to remove calibrations, tests of the C_3F_6 injection system and times that the instrument was malfunctioning.

Many technical difficulties arose over the course of the campaign that needed to be filtered out of the final dataset as well. Data from some nights were removed due to insects getting caught in the GTHOS inlet. Heavy rainfall also resulted in the removal some data. In these cases, rainwater entering the instrument inlet created smaller drops that greatly increased the scattered light and background signals. Power fluctuations leading to unreliable data returns were also removed.

In the case of HO_2 all data prior to the twenty fourth of June was removed from the dataset. Prior to this time, the instrument's NO injection ring sat further away from the measurement axis then it did for the rest of the campaign. While this allowed more time for NO to mix into the sampled airflow and convert HO_2 to OH, it also increased the magnitude of the RO_2 interference in the instrument. Even at the lowest flow of NO, the interference in this configuration was still significant and so these data were removed.

Another correction was applied to the data to account for a malfunctioning zero air generator within the GTHOS platform. The air is used to purge the arms containing the White cell optics and to be a sheath flow that acts to isolate the sampled flow from the detection cell walls. However,

it used a filter that became ineffective much sooner than predicted, causing a steadily increasing interference signal to appear in the GTHOS data. The interference signal was laser-generated and so by varying the laser power this signal could be quantified and removed from the OH data.

2.4 The Regional Atmospheric Chemical Mechanism, Version 2

Over the past two decades, several models have been developed that attempt to describe atmospheric chemistry. Some of these claim to explicitly describe the relevant chemistry like the Master Chemical Mechanism (MCM). However, even in the MCM, many rate coefficients for similar reactions with different VOCs are exactly the same. Because of this, and to cut down on computational expense, some models take a less explicit approach to describing the chemistry. One of these "lumped parameter" models, the Regional Atmospheric Chemical Mechanism Version 2 (RACM 2), was used for the model analysis in this paper.

RACM 2, is an updated version of the original RACM, which itself came from the RADM model and its successor RADM2 (Goliff et al., 2013). The model aggregates organic species into several categories based on how they react with other constituents in the atmosphere. Species that react similarly are placed into the same category and are treated as one chemical type. The model reaction scheme thus uses these chemical types and their reaction products. Given the high isoprene levels expected in the campaign and the need and ability to examine the isoprene mechanism in detail, isoprene chemistry is taken out of the RACM 2 lumped mechanism and is included as explicit reactions in the model. The explicit isoprene mechanism is taken from Paulot et al. (2009).

In order to calculate OH and HO_2, values of other chemical species were set to the measured values when possible in the model thus constraining the model to the other measurements. The specific measurements included in the model run were selected both due to their presence in the RACM chemistry but also for their quality and consistency over the course of the SOAS campaign. Any data which were missing or otherwise unsuitable for integration into the model were removed and an interpolation was used to fill in these missing data. All of the data were then interpolated onto the same time-step of ten minute intervals and organized into the text input files used to run RACM 2.

Because photolysis frequencies (J values) were not measured during SOAS, J values input into RACM 2 were calculated using the NCAR Tropospheric Ultraviolet and Visible Radiation Model (TUV) (Madronich and Weller, 1990). TUV can return calculated J values for 86 different photolysis reactions based on date, time and location. In addition to TUV, other J values needed to run RACM 2 were calculated from the equations used in the MCM.

Both of these methods used to calculate J values assumed clear overhead skies. In order to properly account for the affects of overhead cloud cover, a method of determining JNO_2 based on measurements of solar irradiance was used. This method, described in Trebs et al. (2009) was shown to produce accurate values for JNO_2. By comparing these "measured" values of JNO_2 to the calculated values produced by TUV, a correction factor that varied between 30 and 80 percent of the clear sky J values could be created which was then applied to the other calculated photolysis rates from TUV.

Chapter 3

Laboratory Diagnostics of RO_2 Interference

Several diagnostic tests were conducted prior to the comparison of the SOAS measurements to the model. These tests were performed to better characterize the RO_2 interference signal in the HO_2 measurements. By performing these tests, the data processing programs used for the SOAS data could be adjusted to match the performance of the instrument during SOAS and ensure that the reported numbers were as accurate as possible.

3.1 HO_2 Conversion and RO_2 Interference

As discussed in Chapter 2, Fuchs et al. (2011) found that HO_2 measurements made by converting HO_2 to OH were prone to interference due to conversion of RO_2 as well(reactions 2.4 2.5 2.6).

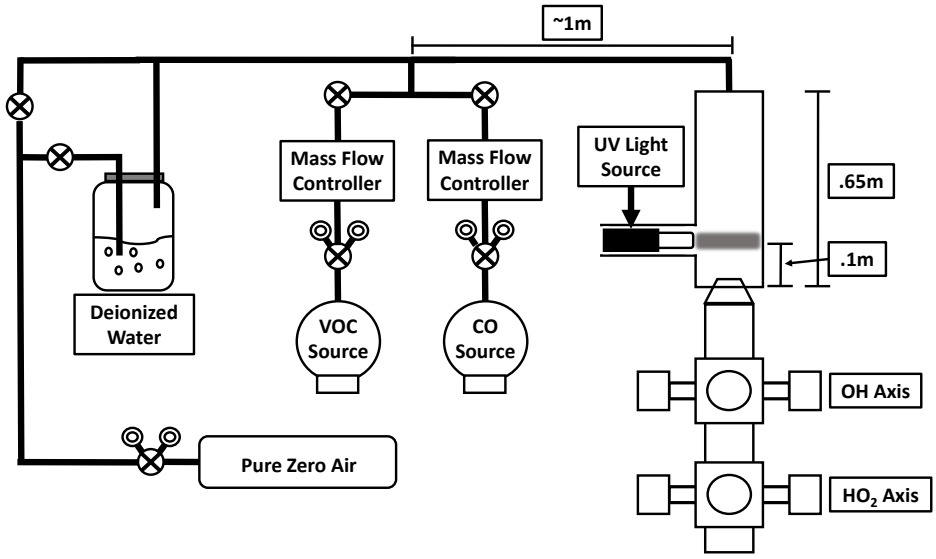

Figure 3.1: Seen here is the setup used to determine the relative signal strength of several common RO_2s seen in SOAS. Humidified air flow is modified by the addition of controlled flow of either a CO mixture or an RO_2 mixture. The combined airflow is passed by a mercury lamp to create a large OH signal which reacts with the other present gas species as they enter the instrument.

To characterize the interference, we determined the efficiency with which GTHOS converts several RO_2s relative to HO_2. To perform the experiment, a flow tube system was added just above the GTHOS inlet (figure 3.1). Pure zero air was flowed through a bubbler and then the moistened air passed by a 185 nm mercury lamp producing OH and HO_2 through the photolysis of water. About a meter before the lamp, gases could be added to the flow via a manifold. First, the conversion efficiency of pure HO_2 was determined for several different NO flows that were used during SOAS (figure 2.3). For this test, carbon monoxide was added to the flow to convert OH over to HO_2. CO was used for this test for its reaction which directly converts OH to HO_2 instead of going through an intermediate step. Based on previous experiments, a ten sccm flow of NO produced the best conversion efficiency for HO_2. The conversion efficiencies of the other flows were then determined based on their relative signal strength to that produced with a 10 sccm NO flow.

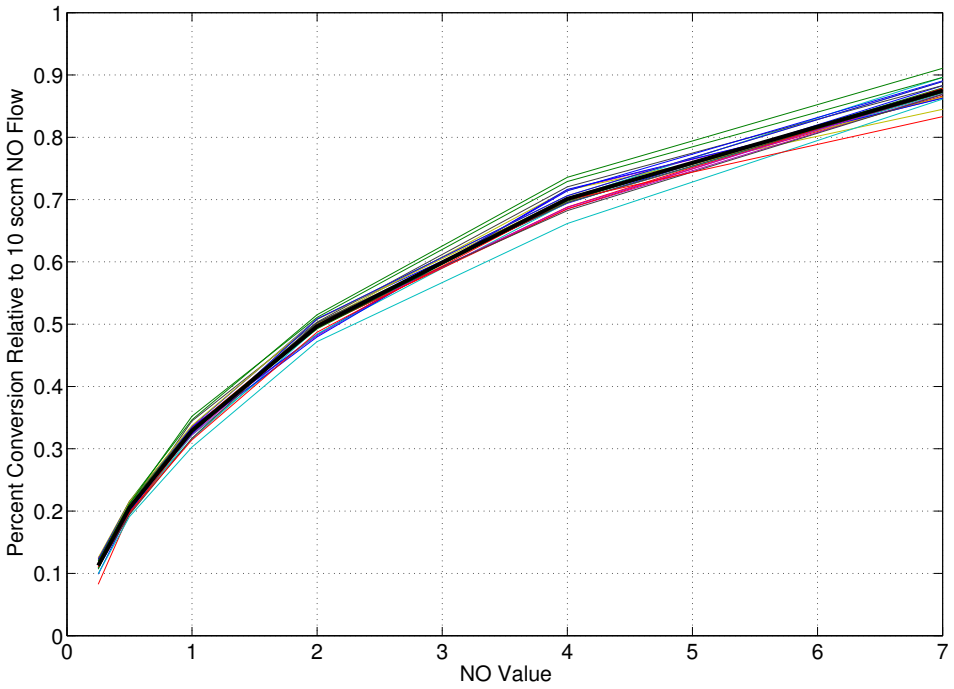

Figure 3.2: Results of the HO_2 conversion tests performed after SOAS. The conversion efficiency for NO flows relative to 10 sccm flow is shown. GTHOS HO_2 calibrations are performed with a 10 sccm NO flow. Thus, 10 sccm is used as a reference value to determine measured HO_2 at lower NO flows.

To find the relative conversion efficiency of the RO_2 species, CO was replaced with several different VOCs, including some believed to be present during SOAS, notably isoprene. The flows of these gases was calculated such that the OH reactivity of the total flow was the same as CO for all trials. The experimental procedure was also the same for all trials. RO_2 conversion efficiency was measured relative to the conversion efficiency of HO_2 for the same NO flow range. The conversion efficiency for each NO flow was then compared to its counterpart in the CO trial. By dividing the two signals, the conversion efficiency of the various RO_2s relative to the conversion efficiency of HO_2 was determined for each flow of NO (figure 3.3).

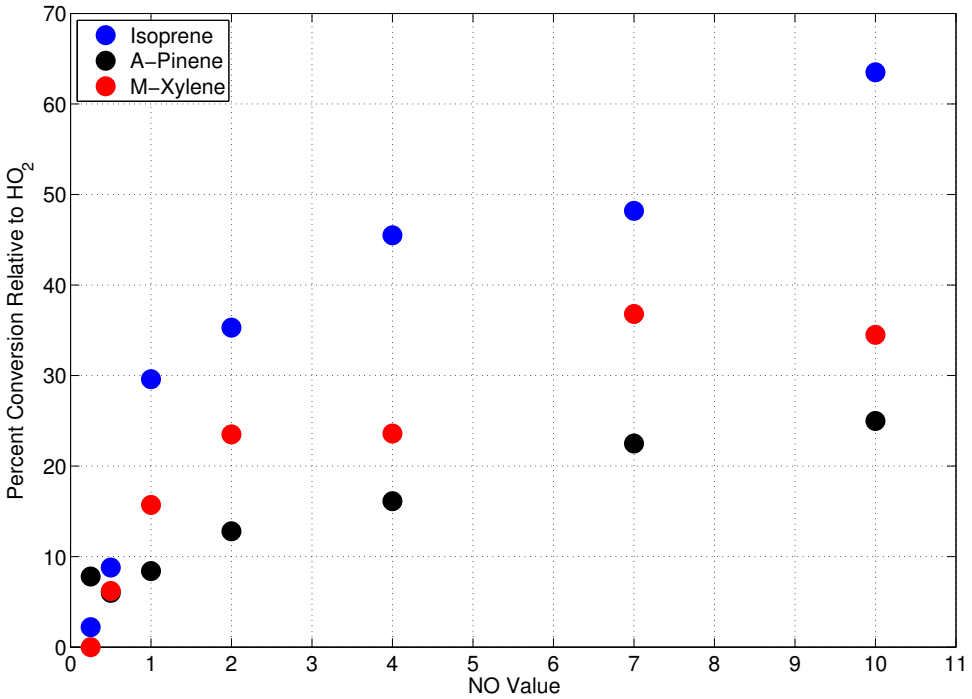

Figure 3.3: Results of the RO_2 interference testing. While the shape of the conversion curves were similar for all of the gases tested, Isoprene conversion had the largest relative magnitude of the potential RO_2 sources. Given its large contribution to SOAS RO_2, the isoprene conversion efficiencies shown here were used to estimate the HO_2 RO_2 interference seen during SOAS.

Ultimately, the relative conversion efficiency of RO_2 was dependent on the NO flow into the instrument. For flows of NO less than one sccm, the relative conversion efficiency for all tested VOCs was below 10%. For higher flows like seven sccm, some VOCs only reached around 30% while other VOCs like isoprene and propene reached relative conversion efficiencies as high as 70%. Given the high concentration of isoprene at the SOAS site, this large conversion efficiency was of particular interest as it implied that HO_2 measured at SOAS was likely significantly affected by RO_2 conversion.

These results are similar to the findings of Fuchs et al. (2011). The paper describes experiments performed to quantify RO_2 interference in a different instrument that also uses NO conversion to OH to make measurements of HO_2. For internal NO concentrations of 1.3 x 10^{14} cm^{-3} isoprene had a relative conversion efficiency of 79%. The authors of the paper came to the same conclusion that isoprene could create a large interference signal in HO_2 measurements made by this method. As seen in Figure 3.3 the relative conversion of RO_2s at a 0.5 sccm NO flow is less than 10% for all tested RO_2 sources. Therefore, reported HO_2 concentrations for SOAS are derived only from times where the flow rate was set to 0.5 sccm. HO_2 data collected for other flows is excluded from reported HO_2.

An interesting result from this experiment is the possibility that the HO_2 measurement axis could be used as a rough measure of ambient RO_2 values in the atmosphere. The NO ramp used during SOAS was on a cycle that averaged at two and a half minutes. By assuming that the HO_2 concentration changes little between 0.5 sccm datapoints, we can find the difference between real

HO_2 and the signal from RO_2. Knowing the conversion efficiency of the different RO_2s by NO, it is possible to approximate the amount of RO_2. To test the plausibility of this theory, we tested this for a case under an assumption that all RO_2 came as a result of isoprene. Given that isoprene was a dominant BVOC during SOAS this is a fairly reasonable assumption to make.

Chapter 4

Results

4.1 Measured OH at SOAS

The measure of OH_{chem} and OH_{int} can be compared to the OH calculated by the model. While the comparison varies day-to-day, the comparison of the median diurnal variation is illustrative (Figure 4.1). As seen in the figure, both measurements seem to follow the same diurnal patterns, but OH_{wave} is consistently higher than OH_{chem}. This result is similar to that of Mao et al. (2012). The removal of OH generated by the external Hg lamp with the chemical method proves that OH_{chem} is the real OH concentration.

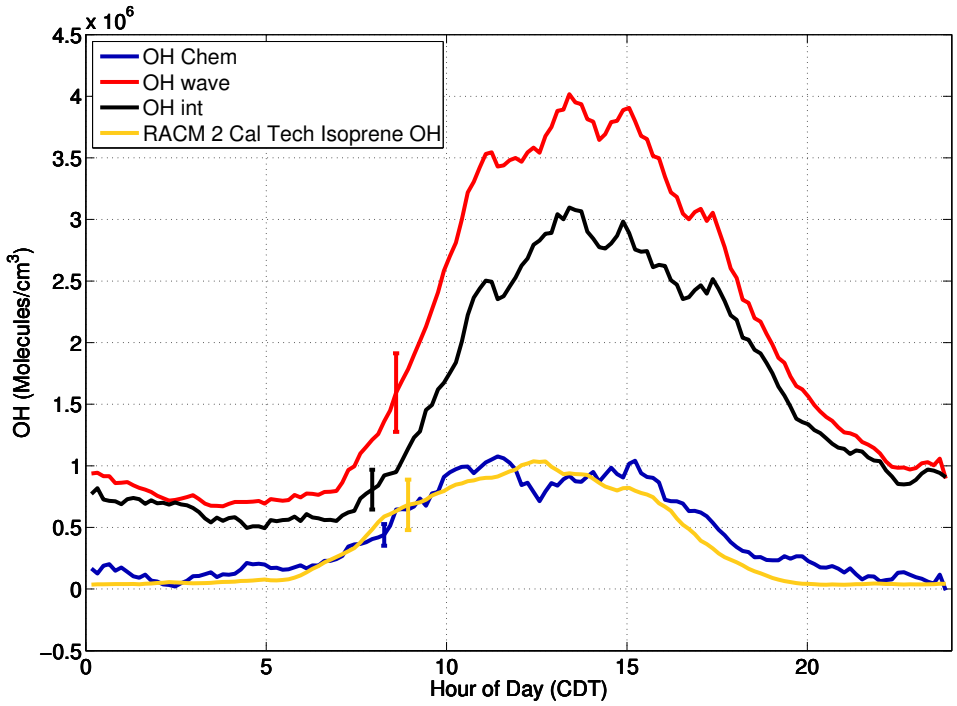

Figure 4.1: Pictured is a comparison of the average diurnal values of OH_{chem}, OH_{wave}, OH_{int} and modeled OH. OH_{chem} has a 2 σ confidence interval of plus or minus 40%. Modeled OH has a confidence interval of $\pm$30%. While both OH measurement methods seem to show the similar diurnal trends, OH_{chem} is consistently lower than OH_{wave} and has a much stronger agreement with modeled values. Comparing OH_{int} and OH_{wave} seems to show that OH_{int} has a strong effect on the behavior of OH_{wave}. A 1 σ confidence interval is represented on this graph.

OH_{int}, the difference between OH_{chem} and OH_{wave} is also plotted in this figure. OH_{int} behaves differently from OH_{chem}, peaking later in the day and persisting longer into the evening hours than OH_{chem} does. OH_{int} also appears to drive the shape and behavior of OH_{wave} more than OH_{chem} does. This difference in diurnal behavior may help to determine the source of this interference in later work.

Model-predicted OH matches well with the measured values of OH_{chem}. The median midday concentration of OH predicted by RACM 2 is 9.0($\pm$2.7)x10^5 molecules cm^{-3} while measured OH_{chem} concentration is 9.3($\pm$3.6)x10^5 molecules cm^{-3}. The modeled to measured ratio is 1.03$\pm$0.3 for OH. The temporal behavior of OH does differ between the modeled and measured values. Modeled OH concentration continuously increases until reaching a daily maximum and then begins decreasing until nighttime. Measured OH plateaus in the late morning and then remains fairly constant through the early afternoon. However, it is likely that these differences are not statistically significant. Midday OH_{int} concentrations are much higher than true OH at 2.7x10^6 molecules cm^{-3}.

4.2 HO_2 Measurements and RO_2 Interference

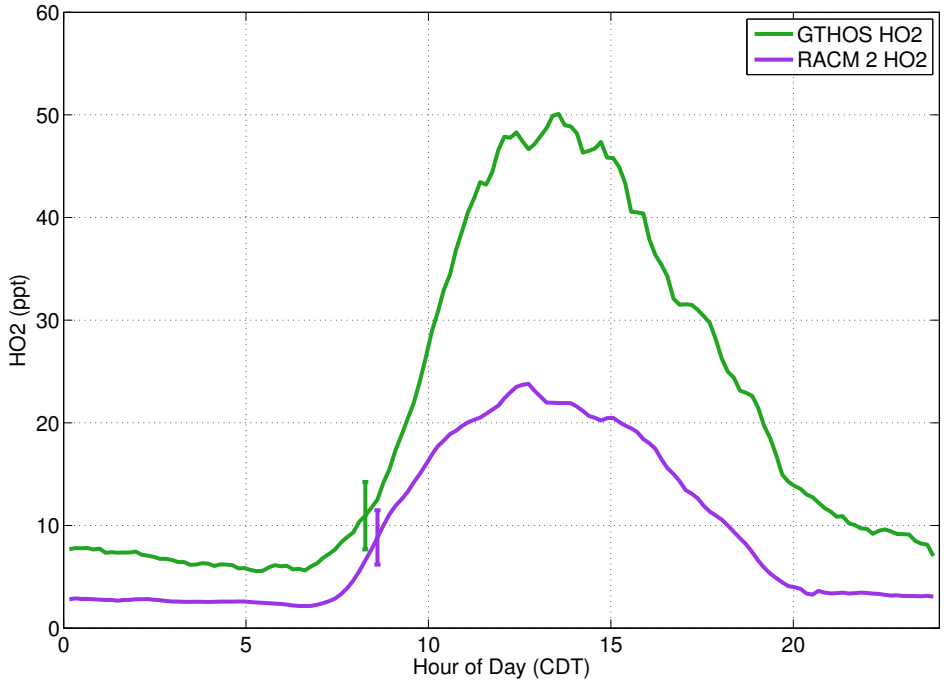

Figure 4.2: HO_2 measurements were greater in concentration than modeled predictions by about a factor of two consistently throughout the campaign. In addition, modeled HO_2 peaks earlier in the day than the measured concentrations. That behavior is easily seen here in this comparison between median diurnal values of the two values. The 2σ confidence intervals for both measurements is $\pm 30\%$.

HO_2 measurements, pictured in Figure 4.2 followed a diurnal trend as would be expected from past measurements. However, when comparing values of HO_2 to model results, there is a considerable discrepancy. Throughout the campaign, measured HO_2, which has a midday average of 46($\pm$14) ppt, are over twice the values predicted by the model output which have a midday average of 20($\pm$6) ppt. Nighttime concentrations for HO_2 saw a lower discrepancy with a measured concentration of 7.4 ppt compared to 2.8 ppt for nighttime averages. However, the ratio between the measured and modeled values remains nearly the same as during the daytime.

This result is similar to the results described in Hens et al. (2013) which also reported a ratio of measured versus modeled HO_2 of almost two. This study also reported good agreement between measured and modeled OH so it is possible that the cause of the discrepancy in modeled HO_2 is related for these two studies. Conversely, Mao et al. (2012) found HO_2 to be over-predicted by the model. Mao et al. (2012) took place over a forest environment where the chemistry was dominated by MBO and pinenes as opposed to the SOAS environment which was dominated by isoprene chemistry. This difference in chemical composition may help to explain why HO_2 was more accurately modeled in that instance.

4.2.1 RO_2 Interference Signal

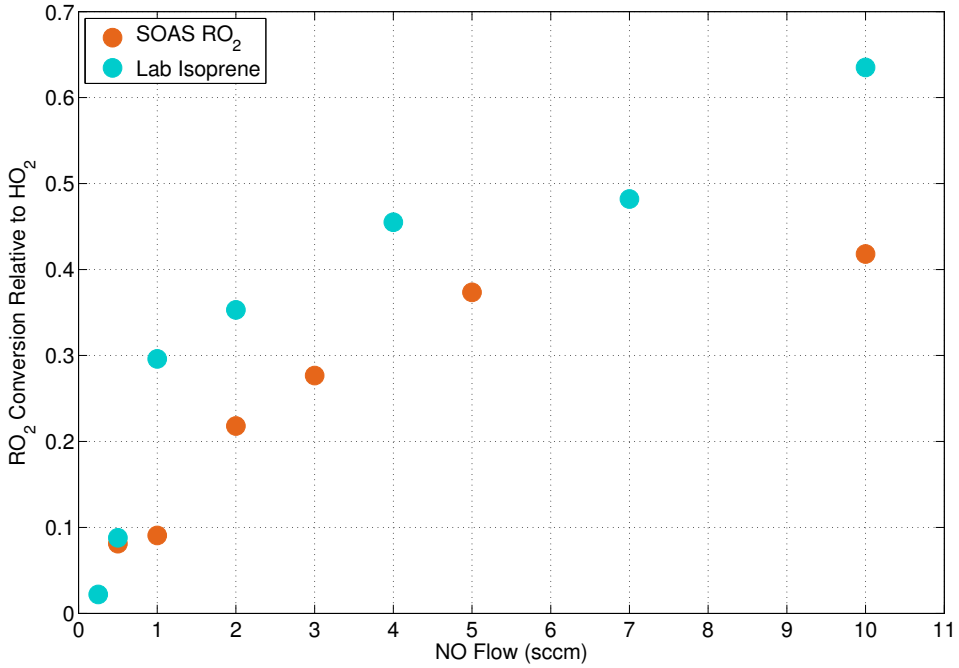

Figure 4.3: Seen here, RO_2 interference as a function of NO flow from SOAS is comparable in shape and magnitude to RO_2 interference due to pure isoprene measured in the lab after SOAS. This result suggests that RO_2 measured at SOAS was primarily due to isoprene based RO_2s.

As discussed in Chapter 3, lab testing was done to characterize the potential RO_2 interference source outlined in Fuchs et al. (2011). This testing determined that measurements taken with the lowest flow of NO into the instrument would be the only ones without the risk of significant interference in reported HO_2. As a result, only these measurements were used to report HO_2 concentration. One advantage of this setup though is that it allows us to characterize the effects that RO_2s are having on the measured values of HO_2. By examining the difference in reported HO_2 signal between measurements at different HO_2 values we can create a chart very similar in shape and form to the one created from the laboratory experiments performed after SOAS.

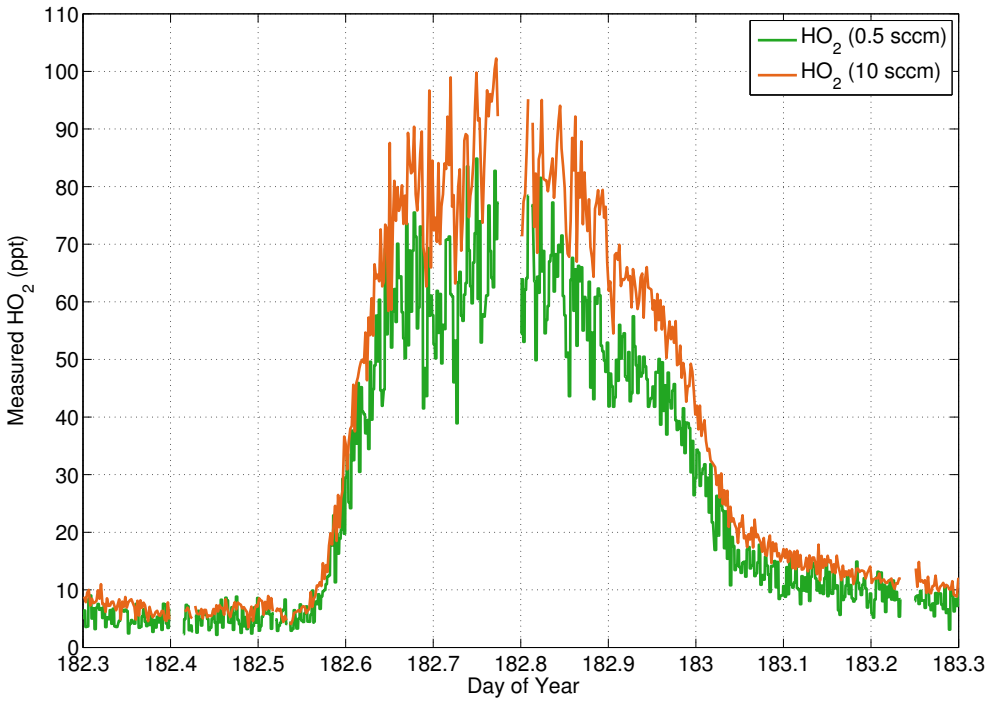

Figure 4.4: HO_2 measurements were greatly affected by RO_2 interference for high NO flows. This is illustrated well in data from July 1. Notice that HO_2 reported by GTHOS is much higher when NO flow into the instrument is 10 sccm.

As seen in figure 4.3 the relative conversion rate of RO_2 is fairly small when flows of NO are small. However, the relative conversion increases notably as the flow of NO is increased, much like the lab results predicted they would. By the time 10 sccm of NO flow is reached, reported HO_2 signals are over 40% greater than the actual ambient HO_2. As shown in 4.4, this discrepancy has an absolute value of only a few ppt during the night time hours when overall HO_2 is low. However, during the daytime hours, this discrepancy can reach as high as 20 ppt for 10 sccm flow of NO. An examination of modeled RO_2 concentrations found that the majority of RO_2 during SOAS came from isoprene based peroxyradicals. Even when combined, the contribution of all other RO_2 sources is low when compared to the isoprene contribution. This result also gives us confidence that subtracting RO_2 from the HO_2 signal based on the isoprene lab results, while a slight over-prediction, was a reasonable decision.

This correction to HO_2 measurements will need to be applied during future field work. However, it could prove to have a few benefits in future work. It is possible that the shape and magnitude of the RO_2 conversion cure could be used to infer the composition of ambient RO_2 present in the local atmosphere and its concentration. However, further work will be required to determine the feasibility and utility of such approximations. In the interim, care should be taken to ensure that this interference does not affect the quality of HO_2 measurements. Pure NO flows of 0.5 sccm or less are the least susceptible, but these low flows could result in uneven NO mixing in the sample. This problem could potentially be avoided in the future if an NO mixture was used. In this configuration, a flow rate could be used that ensures good mixing, without introducing too much RO_2 interference.

4.3 OH Reactivity

OH reactivity calculated from a combination of measured and modeled species failed to match the measured OH reactivity in the field. As seen in figure 4.5, a consistent factor of two difference between the modeled and measured OHR was present throughout much of the campaign. Results like this are not uncommon for forested environments and were recently seen in Hens et al. (2013). However, some campaigns, such as Mao et al. (2012) have had success in accounting for most of the observed reactivity but only after adding OH reactivity from modeled species that were not measured to the calculated OH reactivity using only the measured species.

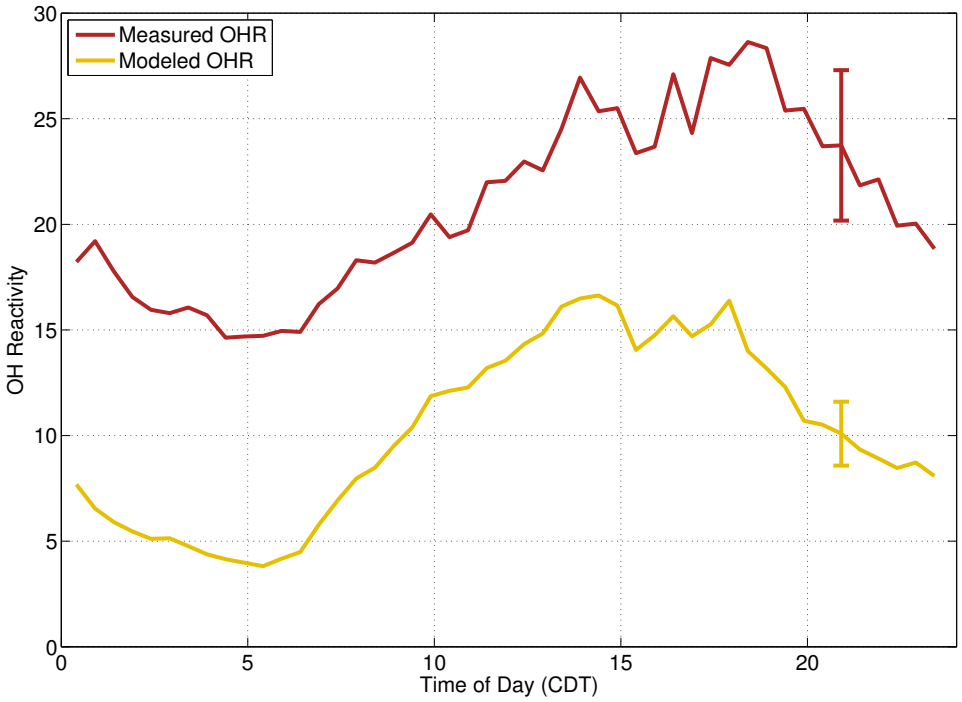

Figure 4.5: Calculated OH reactivity ended up falling well short of the OH reactivity measured during SOAS. This missing reactivity may be due to lacking measurements of RO_2 and may also be related to missing HO_2 in the model.

One possible explanation for this missing reactivity is related to hydrocarbons and isoprene-based RO_2 species that go unmeasured and unaccounted for in the model. This possibility, discussed further, in Hens et al. (2013) may also help to explain the under-prediction of HO_2 by the model. Unrealized species would be highly reactive with ambient OH, helping to fill in the missing reactivity. In addition, these unrealized species would also be able to form more RO_2s which would go on to produce HO_2 by reaction with ambient NO (Equation 2.7), helping to increase HO_2 in the model. Model analysis showed that a large majority of the active RO_2 species during SOAS were products of reactions with isoprene. Thus, it is likely that missing RO species would be isoprene-based as well.

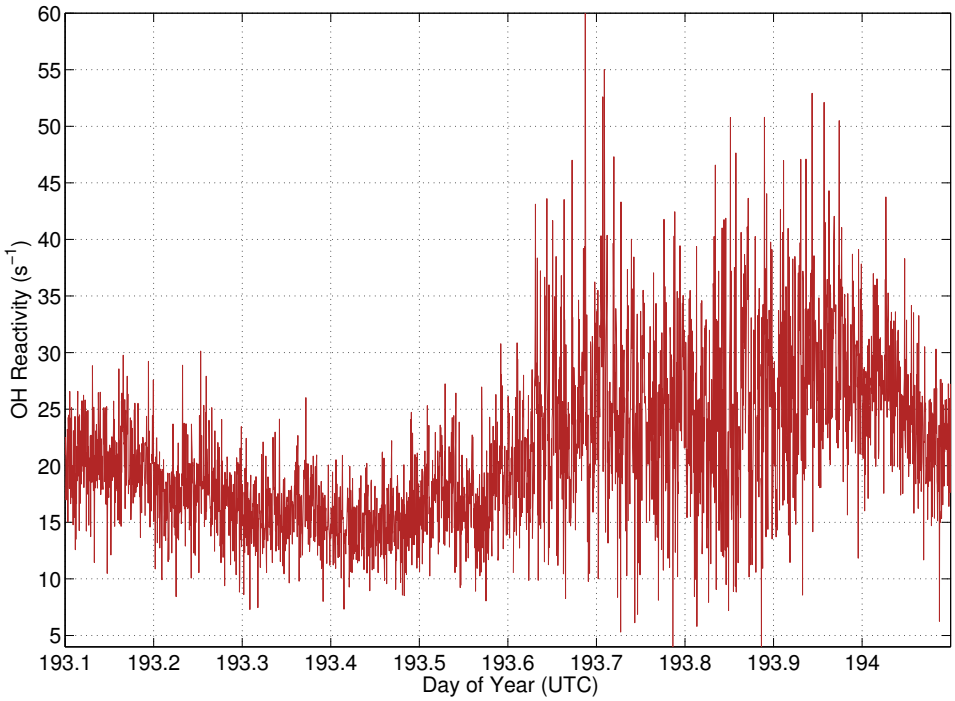

Figure 4.6: OH reactivity measurements were taken at a 30 second resolution throughout SOAS. Measurements from July 12 provide a fine example of OH reactivity variability increasing during the daytime hours, a feature not seen in the time averaged OH reactivity plots used for most analysis.

As seen in Figure 4.6, OH reactivity showed a strong diurnal trend much like OH and HO_2 throughout the course of the campaign. One interesting feature to note however, is the fairly large increase in variability that OH reactivity acquire during the daytime hours. One possible explanation for this behavior is that daytime convective eddies were sometimes lifting highly reactive BVOCs up from the forest canopy, while at other times, sinking air brought relatively clean air from higher up in the atmosphere. However, comparisons between OH reactivity and measurements of other BVOCs like isoprene will need to be made before we can know if this is the cause of the variability for sure.

4.4 HO_x Budget Calculations

To investigate the modeled versus measured HO_2 and OH reactivity discrepancies further, calculations of the HO_x budget for the SOAS campaign were performed. Calculations for both the production and loss of OH and HO_2 were made using reaction equations from RACM 2. Measured values were used in the calculations when available, though model calculated values were used to fill in any chemical species that were not measured during SOAS.

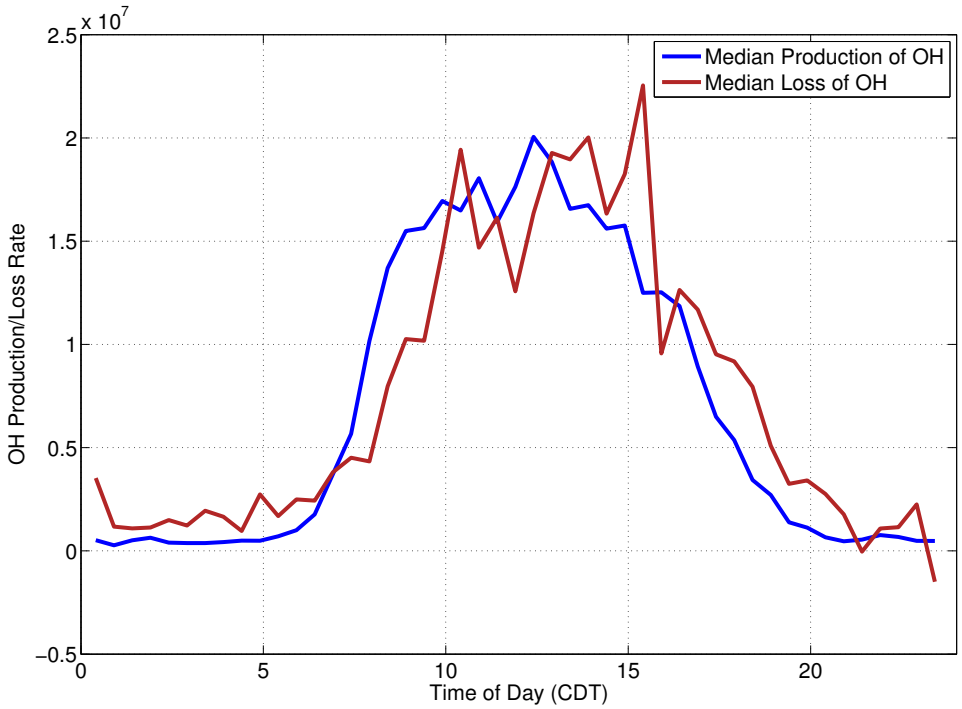

Figure 4.7: Seen here are calculated diurnal averages of OH production and OH loss. The plot shows good agreement between OH production and loss for most times of the day.

The strong agreement between measured values of OH and model calculations is explored in calculations of the HO_x budget for SOAS. As seen in figure 4.7 there is very good agreement between the calculated terms for the production and loss of OH for all times excluding the late morning. However, in the morning, there is a factor of 1.5 discrepancy between production and loss of OH.

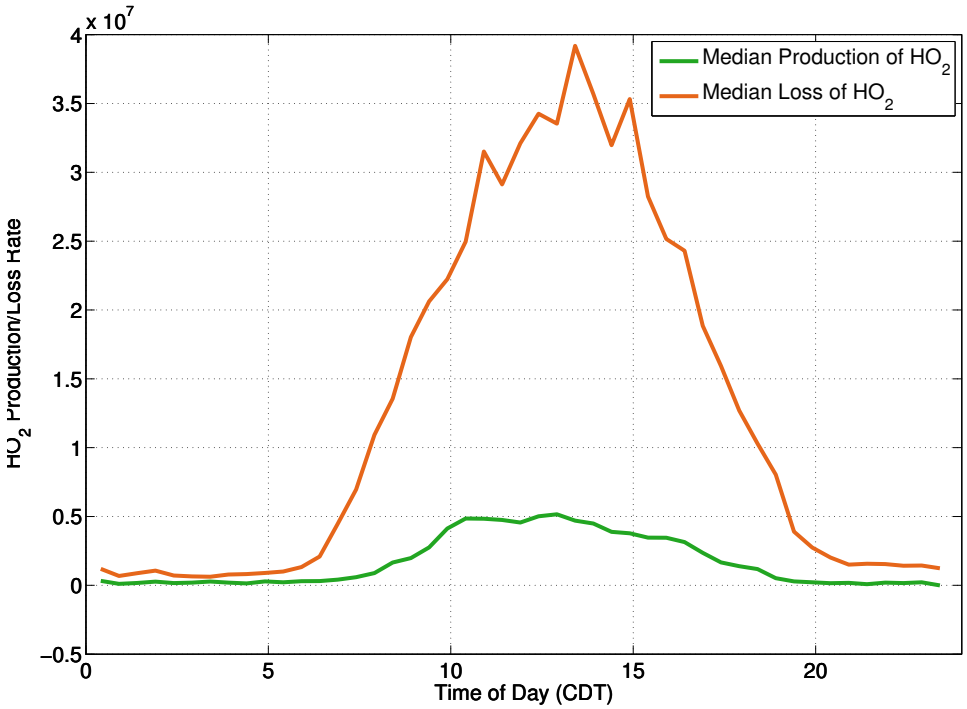

Figure 4.8: Calculations of the daily HO_2 budget, seen here, show that the calculated loss of HO_2 was much larger than its production. This discrepancy could shed light on the under-prediction of HO_2 by RACM 2.

The HO_2 budget showed a much lower level of agreement than OH did. The sink term for HO_2 was consistently about 7 times lower than the production term for the campaign. The fact that the sink term for HO_2 was so much greater than the calculated production term could help to explain why modeled HO_2 was under-predicted relative to the measured values. The presence of additional RO_2, which would lead to additional HO_2, would increase the HO_2 production rate and thus could bring the HO_2 production into closer balance.

4.5 OH Levels Relative to NO_x concentration

Recently Rohrer et al. (2014) suggested that there is a possibility that ambient BVOCs do not suppress OH concentrations as much as previously thought. To support this hypothesis, a plot of normalized OH vs normalized NO_2 was shown with average OH vs NO_2 values from several previous field campaigns plotted in addition to a theoretical curve of how OH concentration should vary with respect to NO_2 based on the current understanding of the chemistry. The OH and NO_2 value at which OH peaks depends strongly on the environment, so to put all the results from different field studies on one curve, the OH value is normalized by dividing by the peak OH value from the theoretical curve and the NO_2 is normalized by the NO_2 value for which OH was maximized in that environment. Thus, the model was run for many different NO_2 values for each environment so the normalized values could all be plotted on one graph

Figure 4.9, a recreation of the original plot shown in Rohrer et al. (2014), shows that measured

OH values tend to agree with model predictions in high NO_x environments like cities, but that most previous studies have found a large discrepancy between modeled and measured OH for low NO_x environments.

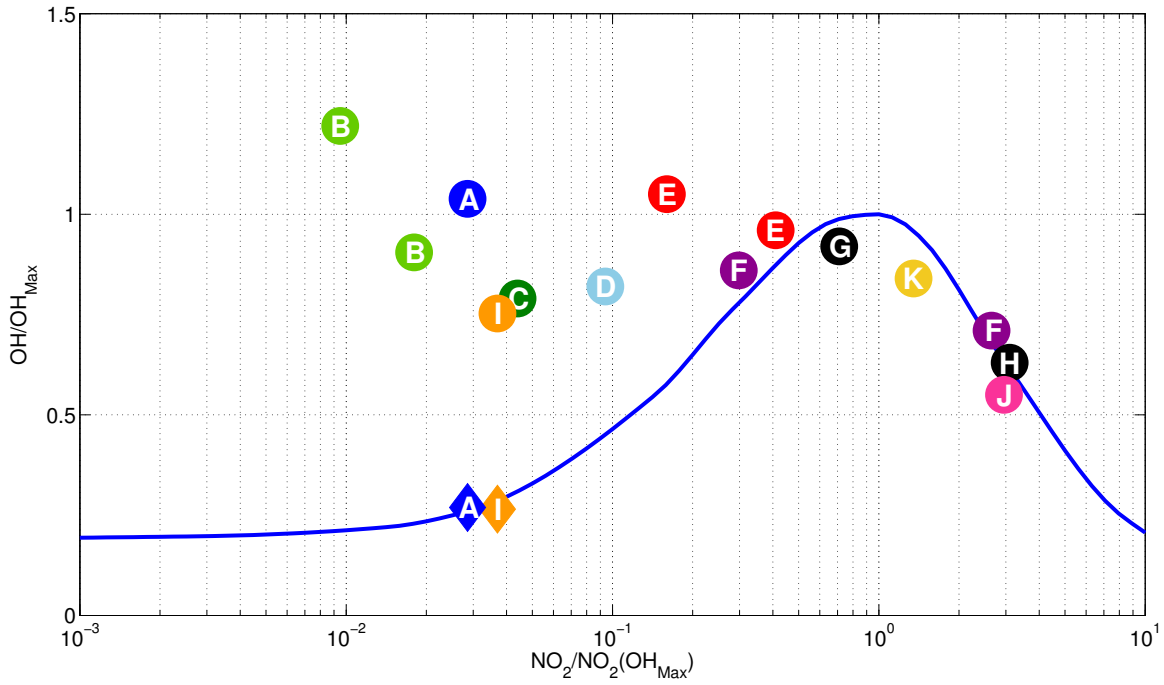

Figure 4.9: This figure, similar to the one seen in Rohrer et al. (2014), shows normalized OH values, compared to increasing NO_2.The plotted line is a theoretical curve of how OH should respond to increasing NO_2 generated from current models. Plotted points are derived from reported data. Circular points represent measurements taken by OH_{wave} like methods while diamonds represent measurements taken by OH_{chem}. Letters denote different field campaigns :A, SOAS; B,Amazon midday and afternoon measurements; C, Borneo; D US deciduous forest; E, Perl River Delta morning and afternoon averages; F, Beijing morning and afternoon averages; G, Mexico City in 2003; H, Mexico City in 2006; I, BEARPEX; J, New York; K, Tokyo. Non SOAS measurements drawn from Rohrer et al. (2014) and references therein

In order to add SOAS data to this figure, a one day dataset was created from the median diurnal values of all of the measurements used to constrain RACM 2 runs. NO_x values being input into the model were then modified to create datasets with NO_x values from 1% to 1000% of the actual measured concentrations from SOAS. The model was then rerun for these scenarios, and a fit was applied to the results to create the smooth curve. Individual points determined from measured results were then added for the SOAS data as well as previous campaigns.

As seen in Figure 4.9, measured values of OH_{chem} are nearly identical to model predicted values of OH. This level of agreement with modeled values is only matched by measurements described in Mao et al. (2012) in the low NO_x regime. Interestingly, these two measurements are the only ones plotted where OH measurements were taken via a chemical removal of OH system. OH_{wave} measurements are also included on this plot for both the SOAS and BEARPEX campaigns. The OH_{wave} results would seem to agree with the other low NO_x results shown in Rohrer et al.

(2014) and would support the conclusions drawn in the paper that unaccounted for recycling of OH is taking place in low NO_x environments. However, the strong agreement between measured OH_{chem} and modeled OH for both the SOAS and BEARPEX campaigns supports the hypothesis that LIF-FAGE instruments have been reporting an interference OH signal in addition to the true OH concentration in low NO_x environments. Such a hypothesis would also imply that OH behavior in forests is fairly well understood, even if there is still a problem.

Given the differences that exist between different instruments used to measure OH by FAGE-LIF methods, it is important to point out that potential interferences in the GTHOS system may not apply to other instruments. However, it is possible that an interference source may be responsible for the large discrepancy that exists between measurements and model calculations of OH in low NO_x environments.

Chapter 5

Summary and Conclusions

Given the prevalence of forested environments around the world, having an excellent understanding of how the local chemistry around them works is vital to developing accurate global chemical models. Past field campaigns in forested environments have reported discrepancies that have led to concerns that forest oxidation chemistry is poorly understood and characterized in models. This has proven especially true in isoprene rich forests where OH measurements have often been well above model predictions. However, these results present the possibility that this chemistry is better understood than previously thought. The addition of the OH_{chem} measurement system to the existing GTHOS instrument has presented evidence that other LIF-FAGE instruments may be subject to a previously unknown interference signal. As was the case with Mao et al. (2012), measurements made by OH chem, show a strong agreement with model predicted OH.

Some have suggested that these processes are being poorly characterized by models and that more effort must be made to improve the isoprene schemes used by them. Rohrer et al. (2014) even suggested that the recycling of OH in forested environments was much greater than previously thought. However, based on the results presented here, chemistry models making use of the mechanisms outlined in Paulot et al. (2009) appear to simulate the observed oxidant levels, at least for OH. Thus, it stands to reason that any global chemical models making use of this chemistry will be able to properly describe the important OH chemistry taking place above the planet's forests.

That said, the chemical model used in this study did struggle to accurately reproduce the HO_2 levels measured in the field. In addition, half of the OH reactivity is missing. As discussed earlier, this may be due to BVOCs and their reaction products. More work will be required to properly resolve the details of these complex reactions.

To confirm the OH findings, it would be ideal if other LIF-FAGE instruments were to install similar chemical method OH measurement systems for their field campaigns. It is also essential that the different instruments be brought together in the same forest for comparison studies. These activities may also shed light on the source of the interference signal potentially seen by other LIF-FAGE instruments. The measurements taken in Hens et al. (2013) made use of such a system and saw similar strong agreement between measured and modeled OH over a forest environment.

In addition, great care must be taken to ensure that RO_2 species do not artificially enhance the reported signal of HO_2, especially in forest environments, where concentrations of RO_2 can approach that of ambient HO_2. This interference can be mitigated by lowering the concentration of NO being used in HO_2 conversion to OH and by limiting the amount of time allowed for mixing of NO and subsequent conversion of RO_2 species. Comparing forest measurements from instru-

ments that use different methods for separating HO_2 from RO_2 is vital to fully understanding this interference.

In the future, different models and specific chemistry schemes should be tested to see how they differ in resolving the aspects of oxidation chemistry. Exploring the strengths and weaknesses of different models and schemes could be helpful in the development of newer more accurate models that would be capable of properly modeling OH, HO_2 and OH reactivity regardless of the environment being modeled.

Bibliography

Di Carlo, P., et al., 2004: Missing OH reactivity in a forest: Evidence for unknown reactive biogenic VOCs. *Science*, **304 (5671)**, 722–725.

Faloona, I., et al., 2000: Observations of HO x and its relationship with NO x in the upper troposphere during SONEX. *Journal of Geophysical Research: Atmospheres*, **105 (D3)**, 3771–3783.

Faloona, I. C., et al., 2004: A laser-induced fluorescence instrument for detecting tropospheric OH and HO2: Characteristics and calibration. *Journal of Atmospheric Chemistry*, **47 (2)**, 139–167.

Fuchs, H., B. Bohn, A. Hofzumahaus, F. Holland, K. D. Lu, S. Nehr, F. Rohrer, and A. Wahner, 2011: Detection of HO2 by laser-induced fluorescence: calibration and interferences from RO2 radicals. *Atmos. Meas. Tech. Discuss.*, **4 (1)**, 1255–1302.

Goliff, W. S., W. R. Stockwell, and C. V. Lawson, 2013: The regional atmospheric chemistry mechanism, version 2. *Atmospheric Environment*, **68**, 174–185.

Hansen, M. C., R. S. DeFries, J. R. G. Townshend, M. Carroll, C. Dimiceli, and R. A. Sohlberg, 2003: Global percent tree cover at a spatial resolution of 500 meters: First results of the MODIS vegetation continuous fields algorithm. *Earth Interactions*, **7 (10)**, 1–15.

Hens, K., et al., 2013: Observation and modelling of HOx radicals in a boreal forest. *Atmos. Chem. Phys. Discuss.*, **13 (11)**, 28 561–28 629.

Kanaya, Y., et al., 2007: Urban photochemistry in central tokyo: 1. observed and modeled OH and HO2 radical concentrations during the winter and summer of 2004. *Journal of Geophysical Research: Atmospheres*, **112 (D21)**, D21 312.

Kovacs, T. A. and W. H. Brune, 2001: Total OH loss rate measurement. *Journal of Atmospheric Chemistry*, **39 (2)**, 105–122.

Lu, K. D., et al., 2012: Observation and modelling of OH and HO2 concentrations in the pearl river delta 2006: a missing OH source in a VOC rich atmosphere. *Atmos. Chem. Phys.*, **12 (3)**, 1541–1569.

Lu, K. D., et al., 2013: Missing OH source in a suburban environment near beijing: observed and modelled OH and HO2 concentrations in summer 2006. *Atmos. Chem. Phys.*, **13 (2)**, 1057–1080.

Madronich, S. and G. Weller, 1990: Numerical integration errors in calculated tropospheric photodissociation rate coefficients. *Journal of Atmospheric Chemistry*, **10 (3)**, 289–300.

Mao, J., et al., 2009: Airborne measurement of OH reactivity during INTEX-b. *Atmos. Chem. Phys.*, **9 (1)**, 163–173.

Mao, J., et al., 2012: Insights into hydroxyl measurements and atmospheric oxidation in a california forest. *Atmos. Chem. Phys.*, **12 (17)**, 8009–8020.

Martinez, M., et al., 2003: OH and HO2 concentrations, sources, and loss rates during the southern oxidants study in nashville, tennessee, summer 1999. *Journal of Geophysical Research: Atmospheres*, **108 (D19)**, 4617.

Mather, J. H., P. S. Stevens, and W. H. Brune, 1997: OH and HO2 measurements using laser-induced fluorescence. *Journal of Geophysical Research: Atmospheres*, **102 (D5)**, 6427–6436.

Monks, P. S., 2005: Gas-phase radical chemistry in the troposphere. *Chemical Society Reviews*, **34 (5)**, 376–395.

Paulot, F., J. D. Crounse, H. G. Kjaergaard, J. H. Kroll, J. H. Seinfeld, and P. O. Wennberg, 2009: Isoprene photooxidation: new insights into the production of acids and organic nitrates. *Atmos. Chem. Phys.*, **9 (4)**, 1479–1501.

Ren, X., et al., 2003a: HOx concentrations and OH reactivity observations in new york city during PMTACS-NY2001. *Atmospheric Environment*, **37 (26)**, 3627–3637.

Ren, X., et al., 2003b: OH and HO2 chemistry in the urban atmosphere of new york city. *Atmospheric Environment*, **37 (26)**, 3639–3651.

Ren, X., et al., 2004: Interference testing for atmospheric HOx measurements by laser-induced fluorescence. *Journal of Atmospheric Chemistry*, **47 (2)**, 169–190.

Ren, X., et al., 2008: HOx chemistry during INTEX-a 2004: Observation, model calculation, and comparison with previous studies. *Journal of Geophysical Research: Atmospheres*, **113 (D5)**, D05 310.

Rohrer, F., et al., 2014: Maximum efficiency in the hydroxyl-radical-based self-cleansing of the troposphere. *Nature Geoscience*, **7 (8)**, 559–563.

Rugters, ????: The southern oxidant and aerosol study website. `http://soas2013.rutgers.edu/`.

Seinfeld, J. H. and S. N. Pandis, 2006: *Atmospheric Chemistry and Physics: From Air Pollution to Climate Change*. Wiley.

Shirley, T. R., et al., 2006: Atmospheric oxidation in the mexico city metropolitan area (MCMA) during april 2003. *Atmos. Chem. Phys.*, **6 (9)**, 2753–2765.

Stevens, P. S., J. H. Mather, and W. H. Brune, 1994: Measurement of tropospheric OH and HO2 by laser-induced fluorescence at low pressure. *Journal of Geophysical Research: Atmospheres*, **99 (D2)**, 3543–3557.

Tan, D., et al., 2001: HO x budgets in a deciduous forest: Results from the PROPHET summer 1998 campaign. *Journal of Geophysical Research: Atmospheres*, **106 (D20)**, 24 407–24 427.

Trebs, I., et al., 2009: Relationship between the NO2 photolysis frequency and the solar global irradiance. *Atmos. Meas. Tech.*, **2 (2)**, 725–739.

Whalley, L. K., et al., 2011: Quantifying the magnitude of a missing hydroxyl radical source in a tropical rainforest. *Atmos. Chem. Phys.*, **11 (14)**, 7223–7233.

White, J. U., 1942: Long optical paths of large aperture. *Journal of the Optical Society of America*, **32 (5)**, 285–285.

Philip Feiner Academic Vita

Graduate Research Assistant: Penn State Department of Meteorology
221 South Barnard St. Apt. 4, State College, PA 16801, 678-778-7844, paf5095@psu.edu

Profile

Integrated Graduate/Undergraduate Student in the Penn State University Meteorology Program. Research focus in collection and data analysis of atmospheric chemistry measurements and models.

Experience

Research Assistant, Penn State Department of Meteorology; Summer 2013-Current
Graduate Research Assistant for the Department of Meteorology. Performing lab work and post field campaign data analysis for Penn State's Ground-based Tropospheric Hydrogen Oxide Sensor (GTHOS). Work also included research with atmospheric chemistry models.

Vice President, Emergency Management Club, Fall 2013-2014
Assisting in development of Penn State Hazard Assessment, GIS hazard mapping and day to day club operations.

Field Researcher, Penn State Department of Meteorology; Summer 2013
Field Research at the Southern Oxidant and Aerosol Study (SOAS) Centreville, Alabama site using the GTHOS instrument

Research Intern, Penn State Department of Meteorology; Summer 2012-Spring 2013
Conversion of the GTHOS instrument from airborne to ground based configuration, calibration and data analysis following the Deep Convective Cloud and Chemistry Project

Meteorological Advisor Intern, Weatherist.com; Summer 2012
Meteorological advisor: helped to develop "Most Probable Forecast" product as well as work on media content creation

Forecaster, On-Air Personality, Penn State Campus Weather Service, 2010-Current
Operational forecasting experience as well as on-air forecasting for the largest student-run campus weather service in the nation

Community Outreach Team Member, Penn State Branch of the American Meteorological Society 2010-2012
Volunteer work educating local community members on various meteorology topics

Skills

Relevant Course Work
Statistics for Geoscientists, Synoptic Meteorology Laboratory, Application of Computers to Meteorology, Remote Sensing, Boundary Layer Meteorology, Graduate Level Atmospheric Chemistry Overview, Introduction to Weather Analysis, Programming for Engineers with C++,

Relevant Course Work (Continued)
Graduate Level Atmospheric Thermodynamics, Climate Dynamics, Geophysical Fluid Dynamics, Advanced Atmospheric Dynamics, Calculus and Vector Analysis

Technical Skills
Programming and data analysis in MATLAB, C++, Perl and IBM's SPSS. Comfortable working in Microsoft, Apple, and Linux workspaces. Proficient with Microsoft Excel, Word, Powerpoint as well as Apple Keynote, Numbers and Pages

Education

The Pennsylvania State University
Schreyer Honors College
Combined Masters/Bachelors Degree
Major in Meteorology, Minor in History
Graduation in December 2014

Honors and Awards

Eagle Scout of the Boy Scouts of America
Awarded February 2010

Scholar of the Schreyer Honors College
Represents the top five percent of students at Penn State. Good standing with the Honors College also confers a yearly scholarship and the opportunity to participate in honors classes and research.

Integrated Graduate/Undergraduate Program (IUG)
Combined study program designed exclusively for Schreyer Scholars who have exceptional academic records; whose progress in the major is so advanced that they would be taking graduate courses in later semesters even without IUG status.

Chi Epsilon Pi
National Honor Society for outstanding students in the field of meteorology/atmospheric sciences. Member since Fall 2012

Dean's List
Awarded for a Semester GPA above 3.5: Fall 2010, Spring 2010, Fall 2011, Spring 2011, Fall 2012, Spring 2013, Spring 2014

Referrals

Dr. William Brune
Distinguished Professor of Meteorology
The Pennsylvania State University
brune@meteo.psu.edu

Dr. Jon Nese
Head of Undergraduate Studies
Senior Lecturer of Meteorology
The Pennsylvania State University
Nese@meteo.psu.edu